Investigation of abradable seal coating performance using scratch testing

Xiao Ma, Allan Matthews

Investigation of abradable seal coating performance using scratch testing

Xiao Ma, Allan Matthews

Department of Engineering Materials, University of Sheffield, Sheffield, S1 3JD, UK

Since the real conditions at the blade tip and the casing in a gas-turbine engine present a complex (very high speed) deformation situation that is difficult and expensive to replicate, we have evaluated the use of a (low speed) standard scratch tester, as a means of assessing the performance of abradable coatings. Three proprietary plasma-sprayed coatings, Ni-graphite, Al–Si-graphite and Al–Si-polyester, were chosen for the tests. The scratch test behaviour was correlated with the mechanical properties of each coating (elastic modulus, microhardness and UTS (ultimate tensile strength)). Our results were compared with those from industrial trials, to ascertain if the scratch test could be used as a relatively cheap and effective alternative to expensive engine trials. We have shown that the "Progressive abradability hardness" (also called "specific grooving energy"), abbreviated below as "PAH", can be utilised as a measure of abradability in the scratch test, and can be related to the mechanical properties, in a manner consistent with engine test-bed findings. We have also found that the abradability and "PAH" can change with scratch length due to coating densification ahead of the slider, which is not easily revealed by other tests (such as the pendulum method). We therefore believe that scratch testing i s a useful means of evaluating the likely in-service performance of abradable coatings, prior to carrying out engine trials.

Keywords: Abradable seal coatings; Scratch test; PAH (Progressive Abradability Hardness); Abradability

1. Introduction

Abradable seal coatings are engineered to minimise the clearance between blade tips and casing to enhance gas-turbine performance [1,2]. As the gas-turbine blades rotate at 3000–10,000 rpm and higher during operation, rotating blade tips may rub the stationary casing, due to either thermal expansion, misalignment or rotation-induced strains [2]. Abradable seals act as sacrificial layers between the blades and the casing, and are soft enough to avoid significant wear to blade tips, thus allowing much smaller clearances. They have achieved great success in both aero-engines and land-based turbo generators [3].

Usually engine makers use high speed rubbing rigs to assess the abradable seal systems by precisely replicating the aero-dynamics and contact environments of the engine [4]; however, such tests are expensive and time-consuming. Attempts to evaluate abradable coatings in laboratory experiments have led to different definitions of coating abradability and a range of evaluation methods. However, a widely accepted method has yet to be agreed on. The paper focuses on the use of a relatively slow deformation rate test, the scratch test, and proposes a convenient indicator of abradability.

2. Experimental

2.1. Materials

Three abradable coating materials were plasma sprayed using standard equipment to Sulzer Metco proprietary spraying parameters. Their compositions (from datasheets) [5–7] are listed in Table 1.

Metco 308NS is based on nickel-graphite cermet powder with a microstructure of a continuous nickel matrix embedded with a graphite solid lubricant and a controlled amount of pores [5]. Metco 313NS uses aluminium silicon alloy-graphite composite powder with microstructure of a continuous aluminium silicon alloy matrix with graphite and porosity uniformly distributed throughout [6]. Metco 601NS is a blend of aluminium, silicon and polyester powder. The microstructure is a continuous aluminium silicon alloy matrix with fairly well-dispersed particles of polyester, which provide abradability and a low friction coefficient [7]. The Metco 450NS bondcoat consists of a nickel–aluminium alloy matrix (80

Table 1
Material chemical compositions and microstructures

Material	Chemical composition (wt. %)				Microstructure (vol. %)		
Metco 308 NS	Nickel 85%	Graphite 15%			Nickel 70%	Graphite 15%	Porosity 15%
Metco 313 NS	Aluminum	Graphite	Silicon	Organic binder	Aluminium–silicon	Graphite	Porosity
	40.0%	45.5%	5.5%	9.0%	70%	22%	8%
Metco 601 NS	Aluminium	Polyester	Silicon		Aluminium–silicon	Polyester	Porosity
	52.8%	40%	7.2%		65%	30%	5%

Ni–20 Al wt.%) and was deposited by thermal spraying to enhance the abradable coating adhesion. Coating materials were sprayed on low alloy steel strips of different sizes. The elastic modulus (E) of the steel strips was 172.4 GPa, and the Vickers hardness was 171 kgf/mm^2.

2.2. Elastic modulus evaluation

A cantilever beam bending test configuration was used in the elastic modulus evaluations of the coatings, using a simple clamping arrangement in a retort stand, with a dial gauge indicator to measure displacement at the end of the specimens loaded with dead weights.

Specimens were grouped with and without bondcoats. Mild steel strip test pieces were coated with the same thickness on both sides. The specimens were then ground to minimise the cross-sectional area variation. Prior estimates of properties were carried out to ensure that the steel strip plastic deformation was avoided, and dead weights of 0.192 kg, 0.384 kg and 1 kg were identified as suitable and applied on each sample. Using standard composite beam theory, the bending behaviour can be used to determine the elastic moduli of the coatings (E_c), as given in Eq. (1):

$$E_c = \frac{4FL^3 - E_s b h^3 y_{\max}}{b y_{\max}(d^3 - h^3)} \quad (1)$$

where F is the dead weight applied on the end, L is the total length of the specimens, E_s is the elastic modulus of the steel substrate, b and h are the width and the thickness respectively of the steel strip and d is the total thickness of the substrate-coating system $y_{\max}$ defines the deflection at the unfixed edge registered by the dial gauge. Note that for the coatings which comprised abradable seal plus bondcoat, a modulus value for the composite coating was obtained. Eq. (1) is developed from the differential equation of the deflection curve [8] and the composite moment–area relation [9].

2.3. Microhardness evaluation

The Vickers microhardness was evaluated using a Mitutoyo model HM-101 microhardness tester. The most widely acknowledged method of measuring the hardness of abradable seal coatings is the R15Y test [7]. This is a "superficial" Rockwell hardness test using a 12.7 mm (0.5 in.) diameter steel ball as the indenter, a minor load of 3 kgf and a major load of 12 kgf. It gives a hardness reading which represents a composite hardness of the coating and substrate. The coating supplier utilised standard deposition processes and materials, for which the R15Y hardness values are given in Table 2. In our studies we wanted to obtain a more localised and precise value for the actual coating rather than the coating and substrate combination. Selected mild steel specimens (of the same geometry as used for the elastic modulus evaluation test) were cut to size, mounted in Bakelite, then ground and polished. Thirty indentations were carried out on each sample face. Each abradable coating was produced in three thicknesses. The indentation loads used, depending on sample material, ranged from 0.01 kgf to 0.2 kgf.

2.4. Ultimate tensile strength evaluation

This test was conducted on a Hounsfield Universal tester. The abradable seal coatings for the UTS tests were plasma

Table 2
Mechanical properties of coating materials

Samples / Properties	Substrate	Metco 450NS	Metco 308NS	Metco 313NS	Metco 601NS	Metco 308NS+bc	Metco 313NS+bc	Metco 601NS+bc
E (GPa)	172.4±9.5	256.5±11.9	3.9±0.7	3.1±0.9	2.1±0.9	4.4±0.6	3.9±0.6	2.7±0.8
H_V (kgf/mm^2)	171.0±6.6	220.1±5.0	33.8±8.0	22.2±6.0	20.6±4.7			
R15Y			65–70	65–75	60–70			
UTS (MPa)			48.6	23.1	8.6			

H_V = Vickers hardness, E = Elastic modulus, bc = bondcoat.

sprayed onto grit blasted mild steel substrates of thickness 1.65 mm, and the coating thickness was 3 mm. Grinding was carried out to avoid cross-sectional area variations.

Defined as the maximum load carried before rupture divided by original cross-sectional. Since the substrate also carries a proportion of the applied load, the ultimate tensile strength of the coating is given by

$$\sigma_{\mathrm{T}} = \frac{L_{\max}}{A_{\mathrm{co}}} = \frac{L - L_{\mathrm{s}}}{A_{\mathrm{co}}} \tag{2}$$

where $L_{\max}$ is the maximum load the coating carries before coating rupture; L is the total tensile load applied by the tester while L_{s} is the load that the substrate carries at that moment. A_{co} is the original cross-sectional area of the coatings, which is 30 mm^2. All the samples were pulled until failure and load-extension curves were recorded by the tester at each 0.02 mm of extension. Since we did not know when this "coating contribution" would reach a maximum (not necessarily when the total load was a maximum), we had to calculate it at each registered time. L_{s} is considered as the yield strength multiplied by substrate's cross-sectional area since substrate yielding was observed prior to coating rupture, therefore substrate work hardening has not been taken into account.

2.5. Scratch test

The scratch tests were conducted using a CSM Instruments Revetest scratch tester. As in the elastic modulus test, the specimens were grouped with and without bondcoats, each having three different abradable seal coatings with a constant thickness of 2.1 mm. All the specimens were mounted flat in bakelite, then polished. The test loading rate was 100 N/min , and the table speed was 10 mm/min.

Five scratch lengths of 0.9 mm, 2.9 mm, 4.9 mm, 6.9 mm and 9.9 mm, were applied , giving final loads of 10, 30, 50, 70 and 100 N, respectively. A data-file recorded the relevant parameters, i.e. normal and tangential force, indenter displacement etc. at each 0.1 mm.

The "progressive abradability hardness (PAH)", elsewhere also termed "specific energy" [10] or, alternatively, "specific grooving energy" [11] (since it is defined as the work done per abraded material volume) , is given by

$$H_{\mathrm{a}} = \frac{W}{V} \tag{3}$$

where H_{a} is the PAH, W is the energy consumed during the scratching process (i.e., the work done by the drawing stylus), V is the groove volume produced. The energy consumed during scratching consists of two components, the indentation work done and the ploughing work done. The terms "work done" and "energy consumed by the indenter" are used with the same meaning in this paper. The point product of the force and displacement define the relevant work done. The scratching process was thus divided into segments each being 0.1 mm, and by summing up the work done within each segment, the total work done was obtained.

Provided the length of the segment is very short as in this case, the forces were assumed constant within one segment. Therefore, considering the ith segment, the ploughing and indentation work done can be described as:

$$W_{\mathrm{P}i} = F_{\mathrm{T}i} \cdot D_{\mathrm{P}i} \tag{4}$$

$$W_{\mathrm{I}i} = F_{\mathrm{N}i} \cdot D_{\mathrm{I}i} = F_{\mathrm{N}i} \cdot (D_{i+1} - D_i) \tag{5}$$

where F_{T} and F_{N} are the tangential force and normal force recorded by the scratch tester, respectively. D_{P} and D_{I} are the ploughing and indentation displacement of the indenter within this segment, respectively, and as mentioned, D_{P} equals 0.1 mm. D is the indentation depth. Parameters of the ith segment are simply denoted by the subscript i.

The total work done can thus be obtained by adding up each segment:

$$W = W_P + W_I = \sum_{i=1} F_{\mathrm{T}i} \cdot D_{\mathrm{P}i} + \sum_{i=1} F_{\mathrm{N}i} \cdot (D_{i+1} - D_i) \tag{6}$$

The groove volume was calculated by summing up volumes of all the segments. A segment volume was considered as an extruded product with respect to the projected indenter profile at the scratch direction, which is a function of the indentation depth. Since each segment's length is rather small, vertical displacement of the indenter within this segment could be neglected and the groove volume can be thus expressed as:

$$V = \sum_{i=1} V_i = \sum_{i=1} A_i(D) \cdot D_{\mathrm{P}i} \tag{7}$$

The profile of the indenter is shown schematically in Fig. 1.

From which it is clear that when the indentation depth is small, the profile is a partial sphere (Fig. 1(a)); when it is large, the profile features the combination of the partial sphere and a trapezoid (Fig. 1(b)). Since all the geometrical features are known, the profile area is a known function of the indentation depth.

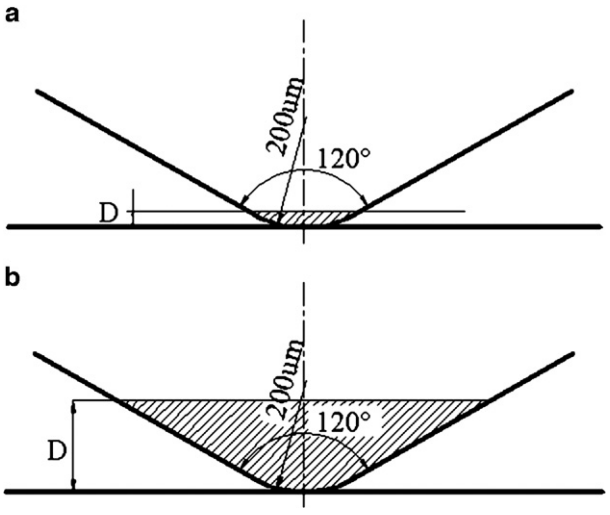

Fig. 1. The scratch stylus profile: (a) The 200 μm radius indenter; (b) The 120° trapezoid.

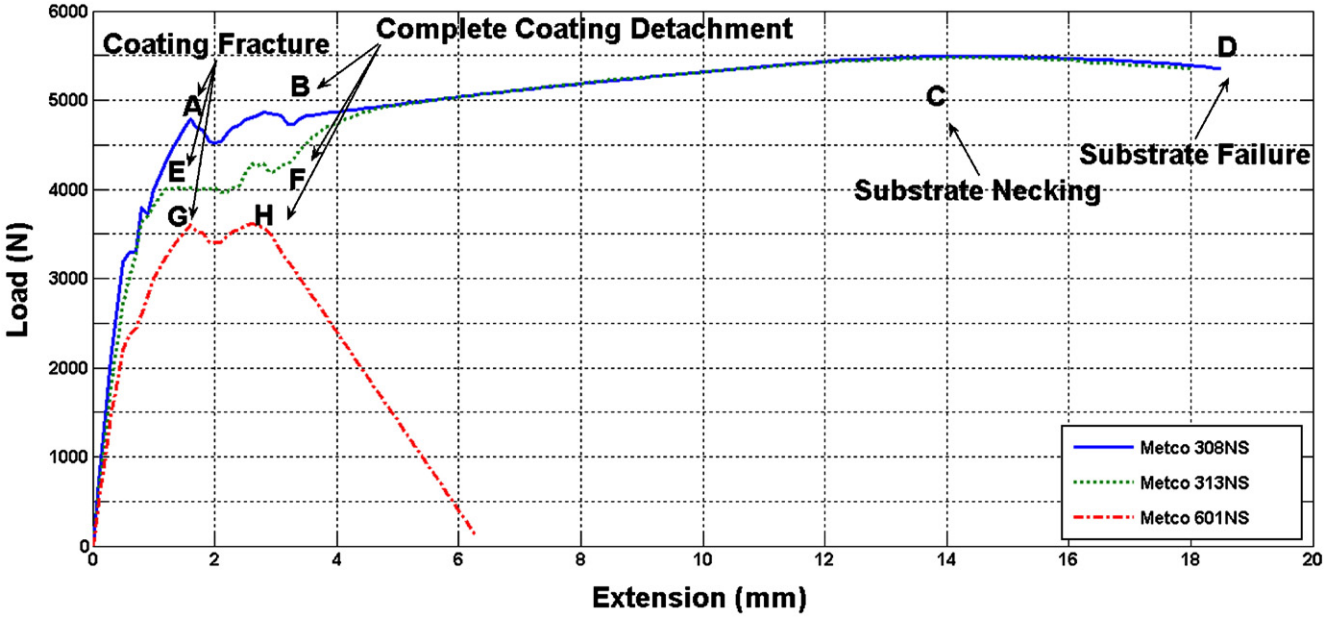

Fig. 2. Load-extension curves in the UTS evaluation.

Therefore, the PAH is described by the following equation:

$$H_a = \frac{\sum_{i=1} F_{Ti} \cdot D_{Pi} + \sum_{i=1} F_{Ni} \cdot (D_{i+1} - D_i)}{\sum_{i=1} A_i(D) \cdot D_{Pi}} \quad (8)$$

All the arguments are as introduced previously. The PAH takes account of the fact that more energy is required to abrade a larger volume of material [10], and has thus been adopted as a measure of scratch resistance in this paper.

3. Results

The results for mechanical property evaluations are shown in Table 2.

The results show decreasing elastic moduli from Metco 308NS to Metco 313NS to Metco 601NS, all of which have extremely low elastic moduli compared to the substrate and the Metco 450NS bondcoat. The microhardness readings of three

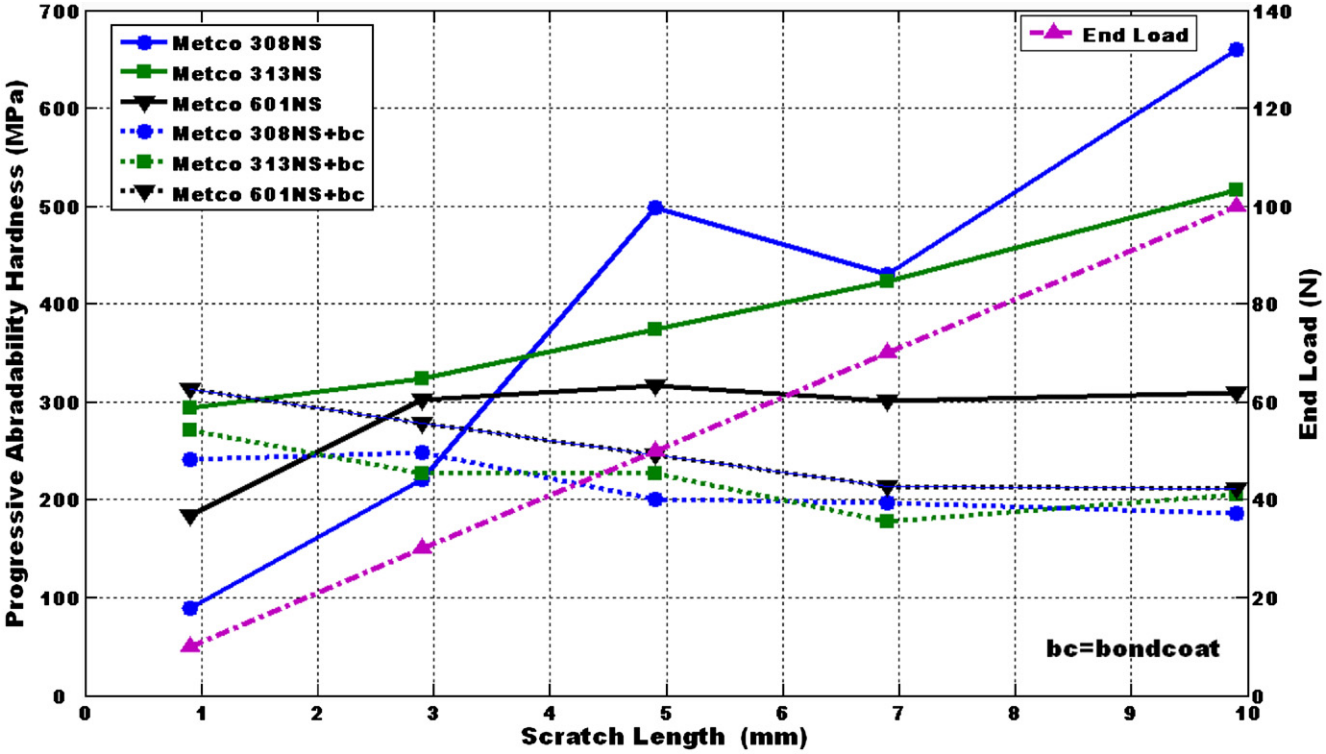

Fig. 3. PAH during scratch test.

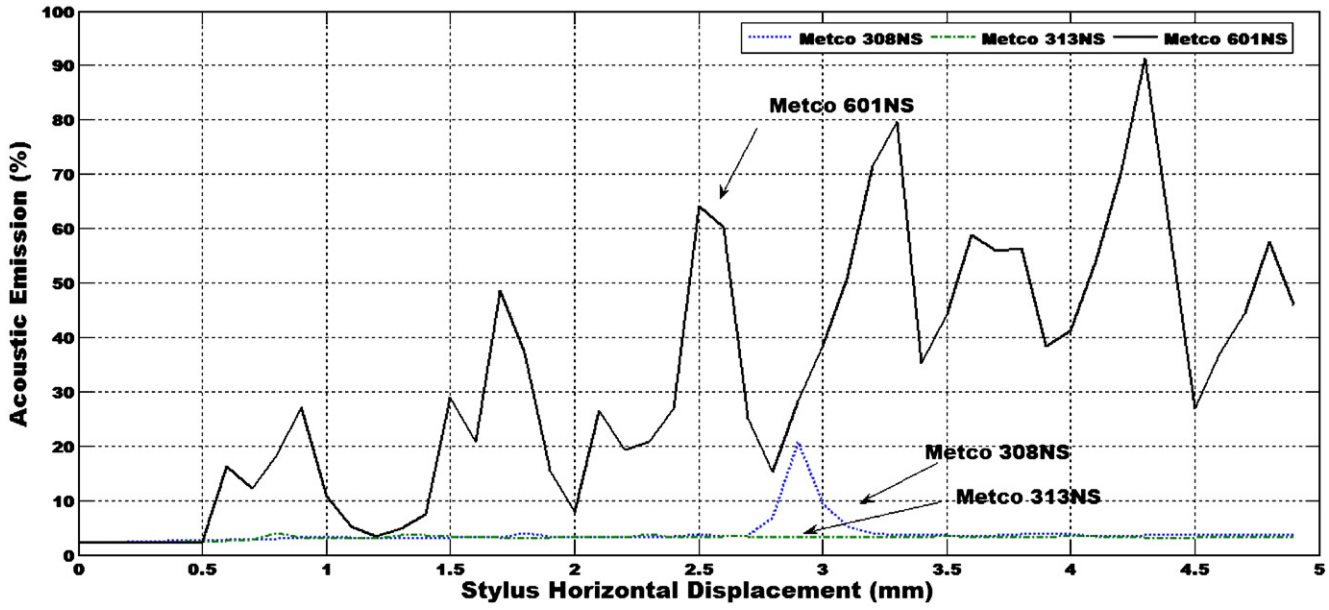

Fig. 4. Acoustic emission of 4.9 mm scratches.

candidate materials varied with the load that was applied. The final microhardnesses were averaged and are: Metco 308NS, 33.8 H_V; Metco 313NS, 22.2 H_V; Metco 601NS, 20.6 H_V. The load-extension curves used for UTS evaluation are shown in Fig. 2. The PAHs of the test samples were determined as mentioned above and are shown in Fig. 3.

4. Discussion

4.1. Elastic modulus evaluation

The abradable seal coatings show extremely low elastic moduli compared to the substrate and the bondcoat. It was observed that at higher loads, the values indicated for the elastic moduli were lower [12]. However, it was also noted that, when higher loads had been applied, the dial gauge did not always rotate back to the exact starting point after the load was released, indicating some permanent plastic deformation of the abradable coating. Although pre-test calculation was performed to ensure that no major plastic deformation would take place, considering the multi-phase structure of abradable coatings, certain phases, i.e. graphite or polyester, might still have plastically deformed under higher loads, leading to this low elastic modulus phenomenon at high loads. Note that the average moduli are indicated in Table 2. It was also found that no dependency between elastic modulus values and abradable coating thickness was evident.

The Metco 308NS and Metco 308NS+Bondcoat samples both exhibited the highest elastic moduli, followed by the Metco 313NS and Metco 313NS+Bondcoat samples, and finally Metco 601NS and Metco 601NS+Bondcoat. A clear increase in the composite coating elastic modulus was introduced by the bondcoat.

4.2. Microhardness evaluation

The microhardness varies with the applied loads. This is most likely due to the fact that the proportion of each phase that was contained in the indentation was not constant and thus they made different contributions to each reading. This is also confirmed by the fact that compared to the bondcoat and substrate, hardnesses of abradable coating materials clearly have larger scatters, which is attributable to uneven microstructure distribution. The Metco 308NS shows a decreasing hardness tendency when tested at higher loads. This maybe be attributable to the indentation size effect whereby lower loads indicate higher hardnesses (due to the large amount of Ni present and hence a greater proportion of elastic recovery in the indentation for smaller indents). Another possible explanation is that there could have been a Ni-enriched layer on top of the sample due to polishing smear, since the large amount of porosity could accommodate this effect. However, indentation positions were carefully selected so that both phases could be sampled, so this mechanism should have a minor influence.

The microhardness decrease from Metco 308NS to Metco 313NS, and finally, to Metco 601 NS, is in line with the elastic modulus decrease.

4.3. Ultimate tensile strength evaluation

The three coatings, Metco 308NS, Metco 313NS and Metco 601NS were observed fracture at points A, E and G, respectively, in Fig. 2, followed by periods of coating detachment up to points B, F, H, and then the subsequent bare substrate necking and failing.

It was found that coating fractures occurred after substrates yielded (see substrate extension in Fig. 2). Also, the load-

extension curves of Metco 308NS and Metco 313NS converge at point B where the Metco 308NS specimen began homogeneous plastic deformation before necking and the coating had been completed detached. Given the substrate yield strength (deduced as 207.5 MPa by analysing substrate tensile strength), it was determined that at points A, E and G , the load carried by coatings reached maximum. The total tensile loads at these points were 4883 N, 4030 N and 3682 N, respectively, and following Eq. (2) the UTS of the coating materials were obtained. The abrupt decline at point H was due to the fact that coating Metco 601NS actually ruptured within one of the grips and the curve went linearly to zero.

4.4. Scratch testing

During the scratch testing no adhesive failure of the coatings was observed. This ensured that the abradability results were not confused by adhesion failures.

Fig. 3 shows the three abradable seal materials and their bondcoat-added counterparts behaved very differently. Since the PAH is defined as the work done per unit volume of material abraded, it takes account of the fact that when the scratch length and indentation depth increase, there is more material abraded requiring more energy input, therefore any increase in PAH reflects a real increase in scratching resistance [10]. The reason for this increase is mainly attributed to densification when the indenter compresses the soft material ahead of it. This may also lead to a work hardening effect. The undeformed material surrounding acts to constrain the deformed volume inside, resulting in a further compressive force that adds to the densification effect. Fig. 3 indicates clearly that Metco 308NS and Metco 313NS underwent densification during the scratching process while the rest did not. The acoustic emission of Metco 308NS and Metco 313NS was less in amount and much smoother than that of Metco 601NS, as shown in Fig. 4 (4.9 mm scratches are selected since this effect is most pronounced in those), illustrating that the major accommodating mechanism in the Metco 308NS and Metco 313NS was plastic deformation. Metco 601NS, on the other hand, with an oscillating acoustic emission, must have experienced a greater amount of fractures, hence showing no apparent densification during scratching.

The Metco 308NS has the highest hardness and the greatest amount of metal matrix content, up to 85% of nickel. Post-facto SEM pictures [12] indicate the metal matrix was compressed and densified under load. Further, the higher yield stress and elastic modulus impart the greatest constraining effect by the material surrounding it, and this adds to the densification beneath the indenter. Another governing effect is that Metco 308NS has the greatest amount of porosity in the microstructure, up to 15 vol.%, which could better accommodate the densification effect. Conversely, the Metco 601NS has the least amount of porosity to accommodate the pressure. Accordingly, the Metco 313NS shows a PAH hardness than Metco 601NS, which has both the lowest microhardness and dynamic hardness values. Therefore, Metco 308NS is considered to have the poorest abradability due to its intrinsic high strength and the undesirable densification, whereas on the contrary Metco 601NS has the best abradability.

The presence of a bondcoat effectively decreased the PAH (i.e. the extent of densification), which was not expected. This is discussed further elsewhere [12].

4.5. Measure of abradability

The PAH is shown to be an appropriate measure of abradability in this paper.

There are a few papers [10,13–15] that state the degree of abradability of an abradable coating material can be related to its measured ultimate tensile strength and/or hardness. The link is also seen in this paper. Metco 308NS has the highest elastic modulus, microhardness and ultimate tensile strength, followed by Metco 313NS and Metco 601NS. Evidently when the hardness, the elastic modulus and ultimate tensile strength increase, the PAH increases as well, signifying a decreasing abradability. Unfortunately, the erosion resistance and abradability are conversely correlated. The optimisation of abradable seal coatings involves the improvement of abradability whilst maintaining the erosion resistance, based on a full insight of the deformation mechanisms. The scratch test, aids understanding on this regard, and is certainly superior to only using hardness as an indicator of abradability.

4.6. Results compared to those from industrial engine test-bed conclusions

It is claimed in datasheets provided by Sulzer Metco Ltd. that the Metco 308NS coating has extraordinary erosion resistance but moderate abradability [5]. This is mainly due to the greater proportion of nickel matrix and the least amount of graphite, combined with the least amount of porosity in its microstructure. The Metco 313NS is claimed to possess a balance of abradability and erosion resistance, and is mainly used in HP compressor seals [6]. It is said to be more abradable than Metco 307NS, and among the Nickel-Graphite group, Metco 307NS is more abradable and less erosion resistant than Metco 308NS. The Metco 601NS [7] is claimed to have a high degree of abradability with essentially no blade-tip wear.

Clearly, the results obtained from scratch tests are in good agreement with conclusions provided by Sulzer Metco Ltd. Although commercial test-bed findings are not available in quantitative detail, Sulzer Metco's datasheets certainly suggest that similar conclusions can be drawn from our scratch testing. The scratch tests indicate that Metco 308NS experienced considerable densification during the scratching and that enhanced its erosion resistance. Metco 308NS was primarily developed for the compressor stages in turbine engines where extremely aggressive particulate matter is present and therefore erosion resistance is crucial [5]. In comparison, the Metco 601NS shows a rather low but stable PAH with virtually no densification taking place, which implies a good abradability but on the other hand it is not an indication of good erosion resistance. The Metco 313NS exhibits moderate PAH and densification halfway between that of Metco 308NS and Metco

601NS, and this could be an indicator of a desirable combination of both good abradability and erosion resistance.

5. Conclusions

1) Results from the evaluations using scratch testing correspond well with test-bed findings of abradability, and this proves that scratch testing maybe an effective alternative, whilst being a relative low cost method.
2) The "PAH" is demonstrated as an appropriate measure of coating abradability, as it is a direct indicator of the ease or difficulty with which the material can be abraded. We have also demonstrated a link with other material mechanical properties such as elastic modulus, microhardness and ultimate tensile strength.
3) The Metco 308NS underwent plastic deformation that led to densification, and it was believed to possess the poorest abradability but best erosion resistance. Metco 313NS was considered to have a good balance between erosion resistance and abradability. Metco 601NS was shown to have the best abradability, but showed a poorer erosion resistance.

Acknowledgements

For assistance in the sample provision the authors would like to express appreciation to Mr. D. Anderson and his staff at Plasma Coatings Ltd. We also thank Dr. J. C. Avelar-Batista Wilson and Dr. J. Housden of Tecvac Ltd. for assisting the authors in carrying out the scratch tests. Thanks also to staff of Rolls-Royce plc. and Sulzer Metco Ltd. for providing useful datasheets concerning the coatings tested.

References

[1] Rolls-Royce plc., The jet engine, 4th edition, Rolls-Royce press, Derby, 1986, p. 245.
[2] AZoM™.com Pty.Ltd, http://www.azom.com/details.asp?ArticleID=739, accessed on 19.08.2006.
[3] P. Dawson, M.S. Walker, A.P. Watson, Seal. Technol. 12 (2004) 5.
[4] R.E. Chupp, F. Ghasripoor, G.D. Moore, L.S. Kalv, J.R. Johnston, 38th AIAA/ASME/SAE/ ASEE Joint Propulsion Conference and Exhibit, Indianapolis, Indiana, July 7–10, 2002, p. 1.
[5] Sulzer Metco Ltd., Technical Bulletin #10-115, 2000.
[6] Sulzer Metco Ltd., Technical Bulletin #10-285, 2000.
[7] Sulzer Metco Ltd., Technical Bulletin #10-141, 2000.
[8] S.P. Timoshenko, M. Gere, Mechanics of Materials, Van Nostrand Reinhold, New York, 1973.
[9] H.S. Zibdeh, M. Abu-Hilah, Eng. Struct. 25 (2003) 397.
[10] Y.N. Liang, S.Z. Li, S. Li, Wear 177 (1994) 167.
[11] F.E. Kennedy, ASME J., Lubr. Tech., 104 (1982) 582–588.
[12] X. Ma, A. Matthews, Evaluation of Abradable Seal Coating Mechanical Properties (Paper submitted to Sealing Technology).
[13] M.A. Clegg, M.H. Mehta, Surf. Coat. Technol. 34 (1988) 69.
[14] F.E. Kennedy, N.P. Hine, ASLE Lubr. Eng. 38 (1982) 557.
[15] M.Z. Yi, J.W. He, B.Y. Huang, H.J. Zhou, Wear 231 (1999) 47.